Chemical Engineering Science 189 (2018) 114–122

Contents lists available at ScienceDirect

Chemical Engineering Science

journal homepage: www.elsevier.com/locate/ces

# $CO_2$ capture from ambient air using hydrated $Na_2CO_3$ supported on activated carbon honeycombs with application to $CO_2$ enrichment in greenhouses

Rafael Rodríguez-Mosqueda *, Eddy A. Bramer, Gerrit Brem

*Department of Thermal Engineering, Faculty of Engineering Technology, University of Twente, Drienerlolaan 5, 7500 AE Enschede, The Netherlands*

## HIGHLIGHTS

- $Na_2CO_3$ loaded over activated carbon honeycombs made cheap and non-hazardous adsorbents.
- $CO_2$ capture occurred in ranges of temperature and humidity representative of ambient air.
- $CO_2$ requirements in closed greenhouses could be fulfilled, replacing fossil fuels.

## ARTICLE INFO

*Article history:*
Received 31 October 2017
Received in revised form 21 May 2018
Accepted 23 May 2018
Available online 26 May 2018

*Keywords:*
$CO_2$capture
Air
Greenhouse
$Na_2CO_3$
Activated carbon
Honeycomb

## ABSTRACT

$CO_2$ capture from ambient air is an interesting option for $CO_2$ enrichment in greenhouses. In this study, adsorbents comprised of hydrated $Na_2CO_3$ supported over activated carbon honeycombs were prepared, characterized and tested for $CO_2$ capture from air. The adsorption of $H_2O$ and the formation of the hydrates were studied by means of FT-IR spectroscopy. The inlet $CO_2$ concentration showed to have a major influence on the conversion yield into $NaHCO_3$, and the results fitted well to the Toth model. A statistical model of the $CO_2$ capture capacity was obtained to get insight into the key parameters of the adsorption process. The air temperature and its moisture content showed to have the largest impact on the $CO_2$ capture, while the flow rate had a minor influence. The chemical reaction path during the $CO_2$ adsorption showed to be determined by the relative humidity conditions inside the reactor. Addition of more salt on the carrier showed to improve the $CO_2$ capture capacity, but this is limited by the strength of the honeycomb carrier. Finally, a preliminary desorption test via a mild temperature and moisture swing was run to assess the feasibility of the process for application in greenhouses. The results showed that the required volume of adsorbent would be roughly 1/1000 of the total volume of a closed greenhouse assuming a target $CO_2$ level of 1200 ppm.



## 1. Introduction

Capturing $CO_2$ from large emitters is probably the most effective action to take in order to mitigate the serious consequences that mankind faces in the near future due to the enhanced global warming effect. Nevertheless, the deployment and application of $CO_2$ capture systems in power plants has not been fast. A complementary action is to extract $CO_2$ straight from ambient air (Sinha et al., 2017; Kulkarni and Sholl, 2012). Although it can be applied everywhere and at any time, its principal drawback lies in the low $CO_2$ concentration, just above 400 ppm. It is possible to obtain valuable products from direct air capture; an interesting option is the use of atmospheric $CO_2$ as carbon source for the synthesis of hydrocarbons, such as methanol, by means of solar energy (Tran et al., 2012; Smestad and Steinfeld, 2012).

Another option could be the production of $CO_2$-enrinched air that can be used for the growth of plants in greenhouses. Running the process with a renewable source or with waste heat streams offers independence from fossil fuel burning. For a fast deployment of this type of capture systems, several characteristics should be considered such as simplicity of the adsorption and desorption steps; easy-to-prepare, non-hazardous and cheap adsorbents. The system should be flexible so that it can capture $CO_2$ in a wide range of temperatures and humidity conditions, as an air pre-treatment step will result in a more complex system, e.g. larger footprint, higher energy penalty, etc.

Different systems have been proposed for the harvesting of atmospheric $CO_2$, the process proposed by Holmes et al. (2013) makes use of a strong hydroxide solution that is regenerated in

* Corresponding author.
*E-mail address:* rf.rodmos@outlook.com (R. Rodríguez-Mosqueda).

https://doi.org/10.1016/j.ces.2018.05.043
0009-2509/

multiple stages. One possible regeneration path is via conventional causticization using lime and an oxy-fired calciner (Holmes et al., 2013). Alternatively, direct causticization at high temperatures using titanium oxide has also been proposed (Mahmoudkhani et al., 2009; Mahmoudkhani and Keith, 2009). Solid adsorbents lead to less complex $CO_2$ capture systems than liquid solutions. Among these, the ion exchange resins proposed by Lackner are comprised of amine groups which chemically trap $CO_2$ (Wang et al., 2011). Some of these resins have shown high capture capacities of around 1.6 mmol $CO_2/g_{resin}$ when treated with 400 ppm $CO_2$ (Shi et al., 2017). Nevertheless, these small particles can impose pressure drop issues since the amount of air that needs to be pumped is very large due to the high dilution of $CO_2$ in it. This is significant for the energy input requirements related to moving the air through the reactor. In this regard, monolithic adsorbents are of special interest due to their very low pressure drop. The highest $CO_2$ capture capacities have been reached with amine-based solid adsorbents (Choi et al., 2011; Choi et al., 2011; Brilman and Veneman, 2013; Chaikittisilp et al., 2011; Belmabkhout et al., 2010; Wurzbacher et al., 2012; Zhang et al., 2014). However, the amount of amine that needs to be loaded onto the carrier is high, and the conversion yields are quite low, below 20% (Sanz-Pérez et al., 2016). Sakwa-Novak et al. (2016) reported an adsorbent comprised of an alumina monolith loaded with polyethylenimine (PEI). The weight loading was 0.3 $g_{PEI}/g_{ads}$ ($g_{ads}$ denotes grams of carrier + grams of PEI) and the maximum $CO_2$ capture capacity was 0.7 mmol $CO_2/g_{ads}$, when treated with a dry gas mixture containing 400 ppm $CO_2$ at 30 °C. Potassium carbonate ($K_2CO_3$) and sodium carbonate ($Na_2CO_3$) react with $CO_2$ forming the corresponding bicarbonate, even at the low $CO_2$ atmospheric levels (Derevschikov et al., 2014; Veselovskaya et al., 2013). $Na_2CO_3$ can form several phases depending on the temperature, water vapor pressure ($P_{H2O}$) and $CO_2$ pressure ($P_{CO2}$). For instance, it can hydrate to produce the mono-, hepta- or decahydrate; the temperature and relative humidity conditions at which some of these transitions happen have been described in detail (Vanderzee, 1982). The monohydrate ($Na_2CO_3{\cdot}H_2O$) is of special interest given the wide range of relative humidities in which it is formed, roughly from 20% RH (relative humidity) to 70% RH at 20 °C. Regarding reactivity with $CO_2$, $NaHCO_3$ or mixtures of this phase with anhydrous or hydrated $Na_2CO_3$ can be formed (Vanderzee and Wigg, 1981). Moreover, $Na_2CO_3$ appears as a cheaper and less hazardous material than the volatile amines.

With respect to the possible application in greenhouses, plant growth rate has shown to be enhanced when the indoor $CO_2$ concentration is increased (Wong, 1990; Pritchard et al., 1999). Doubling or tripling the $CO_2$ concentration indoors is actually a modest raise in the net amount of $CO_2$, making $Na_2CO_3$ an attractive candidate for pumping $CO_2$ from outside into the greenhouse. Furthermore, using $CO_2$ from ambient air gives the possibility to get rid of fossil energy sources for the $CO_2$ enrichment, and to switch to any renewable energy source like solar and wind.

In the present paper, an adsorbent comprised of hydrated $Na_2CO_3$ supported over an activated carbon honeycomb monolith was tested for capturing $CO_2$ from ambient air. First, the adsorption of water by the adsorbent was compared with that of the honeycomb carrier itself. Identification of the phases formed during hydration was investigated. Then, the influence of the inlet $CO_2$ partial pressure on the capture capacity was studied applying the Toth adsorption model. The effects of the adsorption conditions, namely the adsorption temperature (T), the moisture content in the air ($P_w$) and the volumetric flow rate of air (F) on the $CO_2$ capture capacity were studied following a design of experiments method using Minitab® Statistical Software (Version 17). This method allows to reduce the amount of experiments required to elucidate and weight the influence of a given set of factors by applying a statistical analysis to the data gathered, resulting in a statistical model to predict the $CO_2$ capture performance within the ranges of the factors tested. In the context of this work, it can help to identify the extent of the influence of some crucial air properties, such as its temperature and water content during the $CO_2$ adsorption step to propose possible $CO_2$ capture mechanisms. Also, the effect of the air volumetric flow rate is investigated, as it is expected to be the main energy input during the adsorption step.

Moreover, an adsorbent with a higher salt loading was tested to evaluate its influence on the $CO_2$ capture capacity. Finally, the regeneration of the adsorbent via a mild temperature and moisture swing was preliminary studied to test its feasibility.

## 2. Materials and methods

### 2.1. Preparation of the adsorbent

Three adsorbents were prepared for the different tests performed. The carriers used were activated carbon honeycomb monoliths comprised of square channels of 2 mm per side and a wall thickness of 0.7 mm. The monoliths had dimensions of 3 × 3 × 3 cm (11 × 11 channels). The preparation method followed was the same for all the adsorbents. First, the carriers were dried in an oven at 120 °C for 8 h. Then, $Na_2CO_3$ (Sigma Aldrich, ≥99.5%) was dissolved in demineralized water to prepare the solutions for the wash coats. The monoliths were dipped in the solution until no more bubbling was noticed. After removal, the monoliths were manually shaken to remove all excess solution remaining in the channels. Finally, they were calcined in the experimental setup at 170 °C for 1.5 h under a flush of dry $N_2$ to convert the salt into anhydrous $Na_2CO_3$. The salt loadings were calculated from the weight change through the preparation method. The salt concentration of the solutions, the salt loadings achieved and the tests run with each of the adsorbents prepared are shown in Table 1. Further details of the preparation method are given in Table S1 in the Supporting Information. As indicated in Table 1, the tests corresponding to the design of experiments for the study of the influence of T, $P_w$ and F on the $CO_2$ capture were carried out in two blocks. Each block corresponding to a different adsorbent (Na-low-a and Na-low-b), both with similar $Na_2CO_3$ loadings. A third adsorbent with a higher salt loading was prepared (Na-high) aiming to increase the $CO_2$ capture capacity. Also, $CO_2$ desorption via a mild temperature and $P_{H2O}$ swing was tested with this adsorbent.

### 2.2. Characterization of the adsorbents

The samples were analyzed with FT-IR spectroscopy using a Perkin Elmer Spectrum 100 spectrometer equipped with a

**Table 1**
Preparation and tests run with the adsorbents.

| Sample | Wash coat solution [g $Na_2CO_3$/g $H_2O$] | Loading [g $Na_2CO_3$/g ads] | Tests run |
|---|---|---|---|
| Carrier | – | – | $H_2O$ uptake |
| Na-low-a | 0.1 | 0.043 | $H_2O$ uptake |
| | | | Effect of $P_{CO2}$ on capture |
| | | | Design of exp. 1st block |
| Na-low-b | 0.1 | 0.041 | Design of exp. 2nd block |
| Na-high | 0.22 | 0.088 | Effect of salt loading |
| | | | T and $P_{H2O}$ swing desorption |

Universal ATR Sampling Accessory. The surface area of the activated carbon carrier was calculated based on $N_2$ adsorption data collected with a Micromeretics ASAP 2400 apparatus, using the BET theory (Brunauer et al., 1938). The pore volume in the range of diameters from 2 to 300 nm was calculated using the BJH theory (Barrett et al., 1951). X-ray diffraction tests were performed using a PANalytical X'Pert Pro Powder diffractometer equipped with a copper anode X-ray tube; Joint Committee Powder Diffraction Standards (JCPDS) were used for the phase identification.

### 2.3. Experimental setup

The scheme of the experimental setup is shown in Fig. 1. It consists of a reactor (R1) of square cross-section with dimensions 5 × 5 × 20 cm, while the gas is fed at the bottom of it. A plate is placed at the inlet to distribute the flow. The monolithic adsorbent is placed on top of a metal foam to further ensure a uniform flow distribution. Metal foams wrapped in aluminum foil are placed between the adsorbent and the inner walls of the reactor to prevent gas bypassing (see right-hand side of Fig. 1. Two thermocouples are inserted from the top of the reactor and go through the honeycomb at two heights, at the top and bottom parts of the monolith, as depicted on the right-hand side of Fig. 1. The gas stream fed to the reactor varied among experiments from $N_2$ to air with different $CO_2$ contents, either dry or humid. The air stream was prepared by passing dry air at a pressure of 5 bar through column C1, filled with zeolite 13X beads that removed all $CO_2$ in it. The flow coming out of the column was divided in two flows, controlled by means of controllers FC2 and FC3. The water was added by bubbling one of these flows through the water reservoir, kept at a constant temperature. The $CO_2$ (Linde, ≥99.7 vol-%) addition was controlled using flow controller FC1. Before each experiment the gas mixture prepared was left to stabilize, meanwhile exiting the system from valve V1 located just before the reactor. Once the gas mixture measured remained stable, valve V1 was switched, feeding the reactor. The concentration of $CO_2$ and $H_2O$ in the feed stream were measured using sensor S1 (PP Systems SBA-5 $CO_2$) and sensor S2 (Omega HX92A coupled with a thermocouple), respectively. $CO_2$ content in the stream exiting the reactor was measured with sensor S4 (LI-COR LI-820). The humidity content in the stream exiting the reactor was measured at two points: immediately after the reactor with sensor S3 (Omega HX92A coupled with a thermocouple), and after the condensation system by means of sensor S5 (PP systems SBA-5 $CO_2$/$H_2O$). The total volumetric flow rate was measured at the exhaust by means of flowmeter FM (DryCal Mesa Labs Defender 520). Calibration of the $CO_2$ sensors was checked throughout the experimental set.

### 2.4. $H_2O$ uptake of the carrier and the adsorbent

Under real operating conditions the adsorbent will be exposed to various relative humidities, thus it is relevant to assess its water uptake. To study the influence of $Na_2CO_3$, the water uptake of the adsorbent was compared with that of the activated carbon carrier only. The samples were placed in the reactor and heated up to 20, 40 or 60 °C with a feed of humidified nitrogen ($N_2$). The relative humidity (% RH) was set at different values in the range from 0 to 80% RH in both directions, increasing and decreasing. The samples were left to stabilize at each relative humidity. When the $P_{H2O}$ measured at the outlet of the reactor was the same as in the inlet side, the sample was withdrawn from the reactor and it was immediately weighted. The data gathered was fitted to the water adsorption and desorption model proposed for activated carbons by Do et al. (2009). Additionally, a sample of pure $Na_2CO_3$ was treated at 20 °C by flushing it with $N_2$ under different relative humidities in the order: 90% RH, 64% RH and 40% RH. FT-IR spectra were collected after each condition.

### 2.5. Effect of $P_{CO2}$ on the capture capacity

The effect of the inlet $CO_2$ partial pressure on the capture capacity was studied by performing adsorption experiments under different $CO_2$ concentrations, up to 2 vol-%. Prior to each adsorption test, the adsorbent was hydrated at 20 °C and $P_w$ = 14 mbar (60% RH) under 5 L/min of $N_2$. Then, an adsorption experiment was performed at 20 °C, $P_w$ = 10 mbar (43% RH) and the different concentrations of $CO_2$ under a flowrate of 5 L/min of air. After each adsorption test the adsorbent was calcined at 170 °C under 5 L/min of dry $N_2$. The $CO_2$ adsorption data was fitted to the Toth model (Tedds et al., 2011).

### 2.6. Design of experiments. Effect of T, $P_w$ and air flow on the $CO_2$ capture

A design of experiments method was followed to investigate the influence of the temperature (T), water vapor pressure in air ($P_w$) and volumetric flow rate of air (F) on the $CO_2$ adsorption capacity. The tests were divided into two blocks according to the

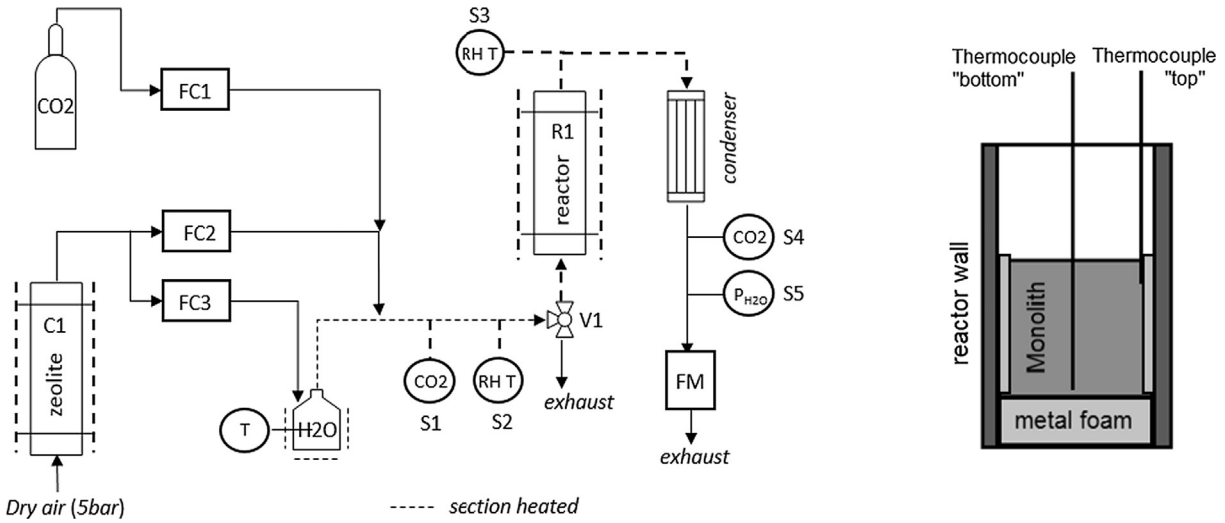


**Fig. 1.** Diagram of the experimental setup (left) and location of the thermocouples inside the reactor (right).

method defined using Minitab® Statistical Software (Version 17). Each block was identified by the adsorbent used (see Table 1).

The approach employed was a surface response since a preliminary linear model showed the presence of curvature in the response of the capture capacity after analysis of the results from the first block. The experimental route consisted in cycles comprised of the following steps: hydration, $CO_2$ adsorption and calcination. The hydration step was carried at 40 °C and $P_w$ = 60 mbar (80% RH) under a flush of 5 L/min of $N_2$ for 2 h. This was long enough to reach the same $P_w$ in the outlet and inlet sides of the reactor. Next, a $CO_2$ adsorption experiment was carried out under 400 ppm $CO_2$. The T, $P_w$ and F factors were varied within the following ranges: temperature from 20 to 40 °C, water vapor pressure from 5 to 17 mbar and the volumetric flow rate from 5 to 15 L/min. The setting with the three factors at their middle values, referred as the center point condition, was repeated six times for the assessment of the repeatability of the results. The adsorption experiments were randomly executed in order to avoid any potential bias. The adsorbent was regenerated by calcining it at 170 °C under 5 L/min of dry $N_2$, it has been reported that $NaHCO_3$ decomposes above 120 °C (Tanaka, 1987). After each calcination, a new cycle was started.

### 2.7. Effect of a higher $Na_2CO_3$ loading and preliminary desorption tests with a temperature and moisture swing

An adsorbent with a higher salt content (Na-high) was used to evaluate its effect on the $CO_2$ capture capacity. The adsorbent was subjected to the same cycling steps as described in Section 2.6. The adsorption conditions tested were only those corresponding to the center point of the design of experiments. The regeneration of the adsorbent was carried out in two steps. In the first step, the adsorbent was set to a temperature and moisture swing at 65 °C with a given moisture content (12 mbar or 75 mbar) under a flush of air containing 400 ppm $CO_2$. The second step consisted on calcining the adsorbent at 170 °C with a flush of dry $N_2$ to completely regenerate it.

## 3. Results and discussion

### 3.1. Preparation and characterization of the adsorbent

As shown in Table 1, the average salt loading achieved for the adsorbents prepared using a solution with a concentration of 0.1 g $Na_2CO_3$/g $H_2O$ was 0.042 g $Na_2CO_3/g_{ads}$ ($g_{ads}$ denotes g carrier + g $Na_2CO_3$). The salt loading increased for the adsorbent prepared with a more concentrated solution, reaching 0.088 g $Na_2CO_3/g_{ads}$ for the Na-high adsorbent. Fig. 2 shows the FT-IR spectra of the activated carbon carrier, anhydrous $Na_2CO_3$ and the Na-high adsorbent after calcination. The carrier showed a baseline drop at low wavenumbers, characteristic of carbon black. Anhydrous $Na_2CO_3$ showed peaks at 1426, 880, 701 and 694 $cm^{-1}$, all these correspond with vibrations of the carbonate. (Buijs and Schutte, 1961) Finally, the spectrum of the Na-high adsorbent was comprised of the bands of these two previous materials, corroborating the loading of $Na_2CO_3$ over the carrier. The BET surface area of the carrier was 729 $m^2/g$. The micropore volume of the carrier calculated with the t-plot method was 0.29 $cm^3/g$, while the total pore volume in the range of diameters from 2 to 300 nm was 0.12 $cm^3/g$, as determined with the BJH method.

### 3.2. Adsorption and desorption of $H_2O$

Fig. 3 shows the water uptake of the carrier and the Na-low-a adsorbent at different temperatures in function of the relative humidity. In both cases the sharpest increase of the uptake occurred at around 50% RH. The presence of the salt resulted on an enhanced water uptake, it was especially steeper at low humidity values, below 50%RH. A hysteresis loop was seen for both samples, although it was wider for the adsorbent. The enhancement of the water uptake in the adsorbent owes to the hydration of the salt. According to previous reports the monohydrate is the only stable hydrate at or above 40 °C (Vanderzee, 1982). Above 80% RH the salt deliquesces, forming a saturated solution (Apelblat and Manzurola, 2003). The experimental data was fitted to the model proposed by Do et al. (2009) for activated carbons, this fitting is represented by the dashed lines. The complete set of fitting parameters for the two samples are given in text T1 in the Supporting Information. Some noticeable differences between the two samples were a smaller water cluster size required for water condensation in the adsorbent, accelerating its water uptake. Moreover, the cluster relaxation constant was also larger for the adsorbent, resulting in more stable water clusters. Consequently, these are maintained at lower relative humidities, broadening the hysteresis loop. Furthermore, the water uptake by the adsorbent was measured at different temperatures; the results showed all to follow the same characteristic curve.

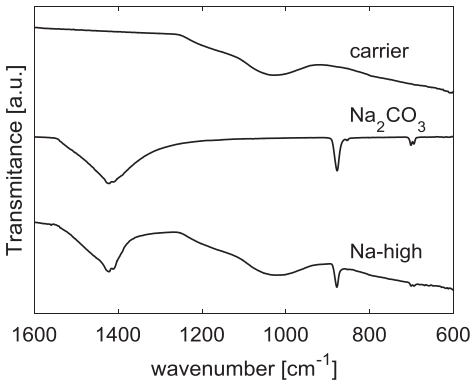


**Fig. 2.** FT-IR of the carrier, $Na_2CO_3$ and Na-high adsorbent.

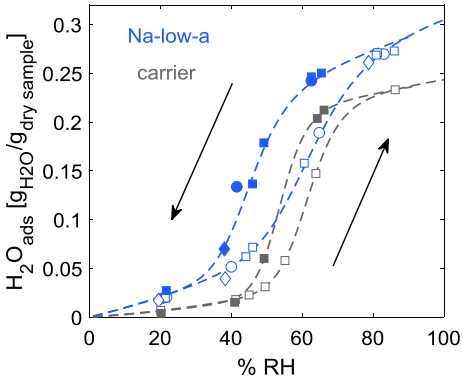


**Fig. 3.** $H_2O$ uptake by the carrier and the Na-low-a adsorbent at (○) 20 °C, (□) 40 °C and (◇) 60 °C. Empty and filled markers are for the increasing and decreasing%RH paths, respectively.

The phase changes of a sample of pure $Na_2CO_3$ at 20 °C are shown in Fig. 4. The spectra after treatments at 90% RH and 64% RH showed very strong bands in the range from 2000 to 4000 $cm^{-1}$, which correspond to water from condensation and /or hydration. The product treated at 40%RH also showed peaks in this range, but of much lower intensity. The wide and strong peak characteristic of the carbonate ion shifted to lower wavenumbers, circa 1379 $cm^{-1}$, for the samples treated at 90% RH and 64%RH. This is in

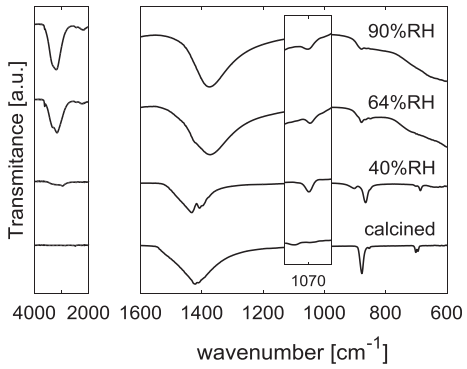


**Fig. 4.** FT-IR of $Na_2CO_3$ after treatment under different Relative Humidity's at 20 °C. The inset shows a zoom at 1070 $cm^{-1}$.

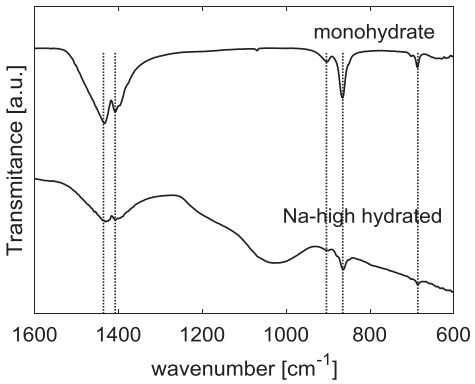


**Fig. 5.** FT-IR of $Na_2CO_3{\cdot}H_2O$ and of Na-high after hydration at 40 °C and 80% RH.

accordance with the spectra reported for the decahydrate and heptahydrate. It has been previously found that only hydrated carbonates show a peak at 1068 $cm^{-1}$ (Buijs and Schutte, 1961). The region zoomed in Fig. 4 shows the presence of this peak in all the samples, except for the calcined sample. Finally, the product treated at 40%RH showed peaks at 903, 866 and 686 $cm^{-1}$, all corresponding to the monohydrate (Buijs and Schutte, 1961). In conclusion, the spectra of each sample after treatment at 20 °C can be assigned to the decahydrate and/or heptahydrate for the products treated at 90% RH and 64%RH and to the monohydrate to the sample treated at 40%RH. Fig. 5 shows the spectra of the Na-high adsorbent after hydration at 40 °C and 80% RH, these were the hydration conditions prior to each adsorption test from the design of experiments set. Opposite to the products at 20 °C Fig. 4, only the monohydrated was formed since neither the heptahydrate nor the decahydrate are stable at 40 °C (Vanderzee, 1982). These results indicate that under average ambient air conditions sodium carbonate will hydrate. The monohydrate appears as the phase stable in the widest relative humidity range, roughly from 20 to 70%RH; thus, it is of interest to study the carbonation behavior of this hydrate for direct air capture.

### 3.3. Effect of $P_{CO2}$ on the $CO_2$ adsorption capacity

Fig. 6 shows the adsorption capacities of the Na-low-a adsorbent at the different $CO_2$ partial pressures tested. Table S2 presents the $CO_2$ concentrations and capture capacities of these tests. The data was fitted to the Toth model, written in equation Eq. (1). (Tedds et al., 2011).

$$n = n_{sat}\left(\frac{(KP_{CO2})^m}{1+(KP_{CO2})^m}\right)^{1/m} \quad (1)$$

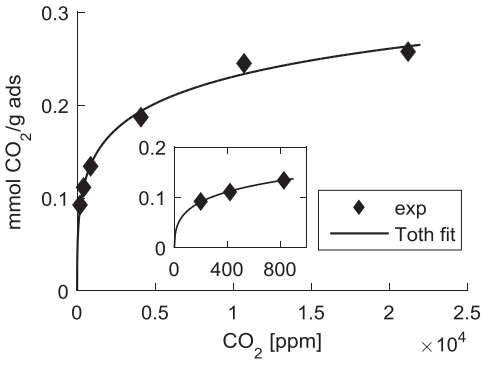


**Fig. 6.** Adsorption capacity versus $CO_2$ concentration. Inset shows the region of low $CO_2$ concentrations.

where $n$ is the $CO_2$ adsorption capacity [mmol $CO_2/g_{ads}$], $P_{CO2}$ represents the partial pressure of $CO_2$ expressed in [ppm], $n_{sat}$ is the adsorption capacity at saturation and $K$ and $m$ are constants retrieved from the fitting. Even though $CO_2$ capture happened via chemisorption, the model seemed to reproduce well the performance of the adsorbent. When extrapolated to 100% $CO_2$ ($P_{CO2}$ = 1 atm), the adsorption capacity calculated was 0.436 mmol $CO_2/g_{ads}$, which is close to the theoretical maximum of 0.406 mmol $CO_2/g_{ads}$ according to the salt loading. The fitted parameter $m$ was equal to 0.16, this accounts for the heterogeneity of the adsorbent sites ($m < 1$ for heterogeneous adsorbents) indicating that the adsorbent was comprised of a wide variety of active sites; the fraction capable of reacting with $CO_2$ decreases with lowering the $CO_2$ concentration. The complete set of parameters resulting from the fit is given in text T2 in the Supporting Information.

### 3.4. Design of experiments. Effect of T, $P_w$ and air flow rate on the $CO_2$ capture

In a real application, the adsorption conditions are determined by the local temperature and humidity. These two air properties are assumed to remain unaltered before entering the reactor. The flow rate through the reactor is a factor that can be tuned during operation. The specific conditions of each test performed and the capture capacities reached are listed in Table S3. Fig. 7 shows the cumulative adsorption capacity for the experiments run at 20 and 40 °C. It was seen that the experiments at lower temperatures favored higher adsorption capacities. This is in line with chemical adsorption being an exothermic process, therefore inhibited with increasing temperature. The highest adsorption capacity of 0.166 mmol $CO_2/g_{ads}$, corresponded to the average of the experiments at 20 °C and 5 mbar under 5 and 15 L/min. A visible difference from the two temperature sets is the separation of the adsorption capacities in function of $P_w$. For the experiments run at 20 °C, increasing $P_w$ had a negative effect on the adsorption capacity. Opposite, at 40 °C, $P_w$ did not seem to have a considerable influence on the adsorption performance as the capacities were very close among each other.

The products from the different $CO_2$ adsorption tests were analyzed with X-ray diffraction, these are shown in Fig. 8. In all cases, reflections corresponding to $NaHCO_3$ were present, nevertheless it is in the reflections from the different type of hydrates where differences are seen. The product from the adsorption at 20 °C and 5 mbar $H_2O$ showed reflections of the monohydrate. The product from the adsorption at 20 °C and 17 mbar $H_2O$ presented the most intense reflections of the hydrated phases: monohydrate and decahydrate. On the contrary, the experiments performed at 40 °C, either under 5 or 17 mbar $H_2O$, did not present reflections corresponding to any hydrated phase.

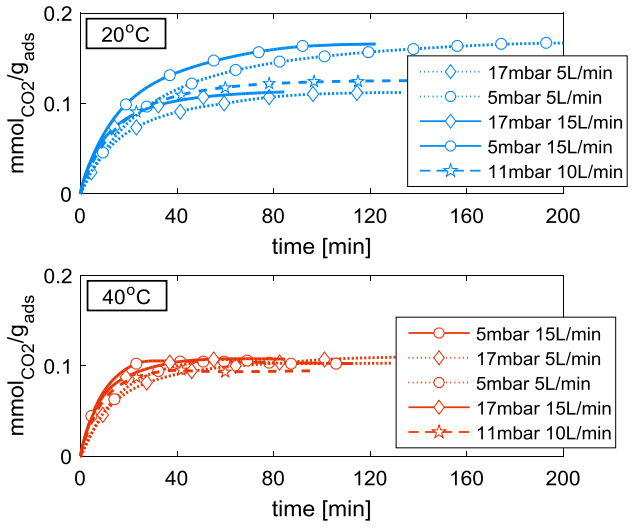


**Fig. 7.** Cumulative adsorption capacity for the experiments at 20 and 40 °C.

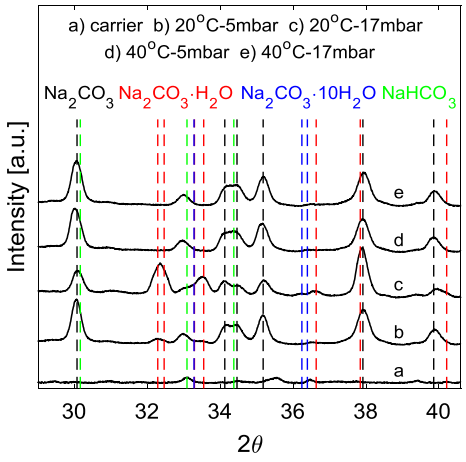


**Fig. 8.** XRD of the carrier and of the products from the $CO_2$ adsorptions at the different T and $P_w$ conditions.

Based on the results from the X-ray diffraction analysis, the suggested chemical reaction paths are:

At 20 °C and 5 mbar $H_2O$(22 %RH)

.

$$Na_2CO_3 \cdot H_2O + CO_{2(g)} \rightarrow 2NaHCO_3 \quad (R1)$$

At 20 °C and 17 mbar $H_2O$(73 %RH)

.

$$Na_2CO_3 \cdot H_2O + 9H_2O_{(g)} \rightarrow Na_2CO_3 \cdot 10H_2O \quad (R2)$$

$$Na_2CO_3 \cdot 10H_2O + CO_{2(g)} \rightarrow 2NaHCO_3 + 9H_2O_{(g)} \quad (R3)$$

At 40 °C and 5 or 17 mbar $H_2O$(7 and 23%RH, respectively)

.

$$Na_2CO_3 \cdot H_2O \rightarrow Na_2CO_3 + H_2O_{(g)} \quad (R4)$$

$$Na_2CO_3 + CO_{2(g)} + H_2O_{(g)} \rightarrow 2NaHCO_3 \quad (R5)$$

These paths explain the differences seen with respect to $P_w$ at the two temperatures in Fig. 7. At 20 °C and 5 mbar $H_2O$, the carbonation of the monohydrate is not directly influenced by water (reaction R1). At 20 °C and 17 mbar $H_2O$ further hydration towards the decahydrate is favored; moreover, the carbonation reaction of this phase is negatively affected by the presence of water (reaction R3). For the experiments at 40 °C, the monohydrate is not stable and it decomposes into the anhydrous carbonate. The carbonation reaction of the anhydrous carbonate requires of water (reaction R5), actually the experiments under 17 mbar $H_2O$ performed slightly better than at 5 mbar $H_2O$, with a mean capacity of 0.108 and 0.102 mmol $CO_2/g_{ads}$, respectively. Nevertheless, this higher adsorption temperature plays a significant role on reducing the $CO_2$ capture performance.

### 3.4.1. Statistical analysis

As the salt loadings of the Na-low-an and Na-low-b adsorbents were not identical, the capture capacity data used for the statistical analysis was normalized with respect to the amount of salt loaded in each sample rather than with the total adsorbent mass. Otherwise, the effect of a different salt loading would have been wrongly attributed to the T, $P_w$ and F factors. The normalized capture capacity is denoted as *capn* and it is calculated as *capn = cap/salt load*, where *cap* is the $CO_2$ adsorption capacity [mmol $CO_2/g_{ads}$] and *salt load* is the weight loading of $Na_2CO_3$ in the adsorbent [$g_{Na2CO3}/g_{ads}$] (see Table 1). The units of *capn* are [mmol $CO_2/g_{Na2CO3}$]. The statistical model resulting from the analysis is given in equation Eq. 2. The input parameters are expressed in: T [°C], $P_w$ [mbar] and F [L/min].

$$capn = 4.7710 - 0.0024T^2 - 0.0031P_w^2 + 0.0073F^2 + 0.0433T - 0.1514P_w - 0.1518F + 0.0058TP_w \quad (Eq.2)$$

The standard deviation of the model is 0.0530 mmol $CO_2/g_{Na2CO3}$, which represents 2% of the lowest *capn* measured; and $r^2$ = 99.1%, indicating a good fit. Fig. S1 in the Supporting Information shows the normalized capacity of the six experiments run at the center condition for both adsorbents. Fig. 9 shows the contour plot for the capacity, converted into the more conventional units [mmol $CO_2/g_{ads}$], in function of T and $P_w$ for a constant value of F = 5 L/min.

### 3.4.2. Effect of each factor on the $CO_2$ capture performance

In order to quantitatively compare the effect of each factor on the capture performance, the derivatives of the normalized capacity with respect to each of them are presented in the next equations.

$$\frac{d\ capn}{dT} = 0.0433 - 0.0048\ T + 0.0058\ P_w \quad (Eq.3)$$

$$\frac{d\ capn}{dP_w} = -0.1514 - 0.0062\ P_w + 0.0058\ T \quad (Eq.4)$$

$$\frac{d\ capn}{dF} = -0.1518 + 0.0146\ F \quad (Eq.5)$$

As it is seen, each of the derivatives includes its corresponding factor in the expression, evidencing the curvature of the response. Moreover, the interaction between T and $P_w$ makes that the temperature at which curvature occurs is defined for each $P_w$, according to Eq 3. This effect is illustrated in Fig. 10a, where %RH is plotted instead of $P_w$ as this is a more practical parameter. At a given temperature of adsorption, increasing %RH will have a positive effect on the $CO_2$ capture up to a certain value till the solid line. Further increase above it will be negative for the $CO_2$ capture. According to the chemical reactions paths proposed previously (R1 to R5), the only phase that is favored by the presence of water

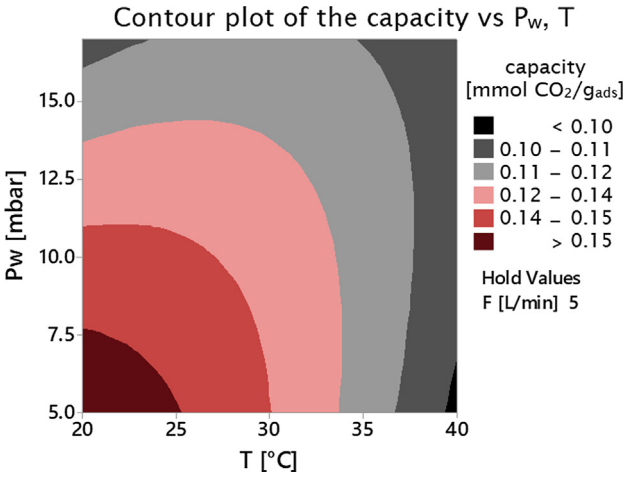


**Fig. 9.** T-$P_w$ contour plot of the capture capacity, holding F = 5 L/min. This plot applies to an adsorbent with a salt loading of 0.042 $g_{Na2CO3}/g_{ads}$. Figure obtained with Minitab (version 17).

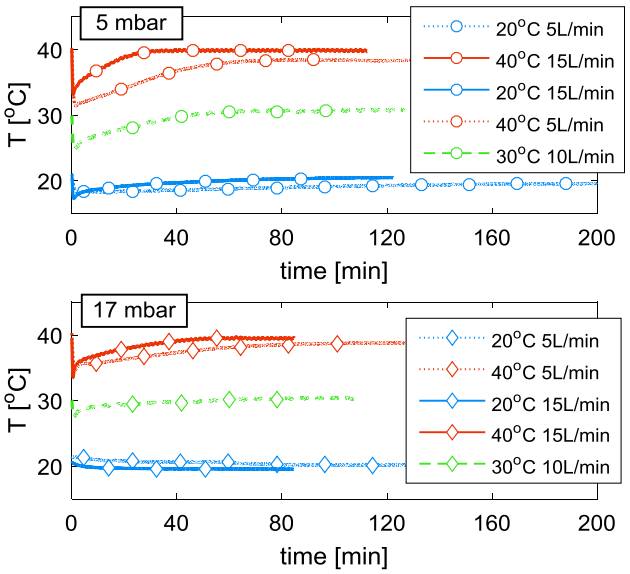


**Fig. 11.** Temperature at the "bottom" location of the adsorbent for experiments at 5 mbar and 17 mbar.

is the anhydrous $Na_2CO_3$, as denoted in reaction R5. The dotted line in Fig. 10a represents the theoretical %RH for the transition between the monohydrate and the anhydrous carbonates, calculated using HSC Chemistry 5.1 software. The fact that the solid and dotted lines don't overlap can be partly explained due to a cooling effect seen in the adsorbent, explained in detail in Section 3.5, which leads to a higher %RH locally that prevents the formation of the anhydrous carbonate. Fig. 10b shows the variation of the capture capacity at different temperatures and %RH.

### 3.5. Evolution of the temperature during the $CO_2$ adsorption

Fig. 11 shows the temperature measured at the "bottom" location of the adsorbent during the $CO_2$ capture. In most cases a cooling effect is seen, which can be explained by looking at Fig. 3 for the adsorbent. Since the hydration treatment prior to each adsorption experiment was performed at 80%RH, water evaporation will take place during the subsequent adsorption test depending on the relative humidity. The larger the difference between the initial $H_2O$ load and the equilibrium uptake at the %RH during the $CO_2$ adsorption experiment, the more water that will be evaporated from the adsorbent, inducing a local cooling. This explains why the largest temperature drop from 40 °C to 31 °C occurred at the condition of 40 °C and 5 mbar (7%RH), while for the case of 20 °C and 17 mbar (73%RH) no appreciable temperature drop happened.

Fig. S2 shows the water vapor pressure measured at the outlet of the reactor during the $CO_2$ adsorption tests.

This cooling effect is an important characteristic of the adsorbent as it buffers the influence of a higher air temperature, subsequently improving the adsorption performance. Fig. 12 illustrates this effect for the Na-high adsorbent, where the capacity of the non-hydrated sample was almost half of the hydrated one. Fig. S3 shows the evolution of the temperature during those adsorption experiments. In a real application, the desorption step can be performed by means of a mild temperature and moisture swing, leaving the adsorbent loaded with water that can act as a coolant in a subsequent adsorption step.

### 3.6. Preliminary analysis for application in a greenhouse

Closed greenhouses can control the inner climate independently of the outside weather conditions. Moreover, less net amount of $CO_2$ is required since cooling is provided inside the facility rather than through ventilation with outside air, which greatly dilutes the $CO_2$ inside (De Gelder et al., 2012). Furthermore, closed greenhouses have shown to lead to an improvement on the

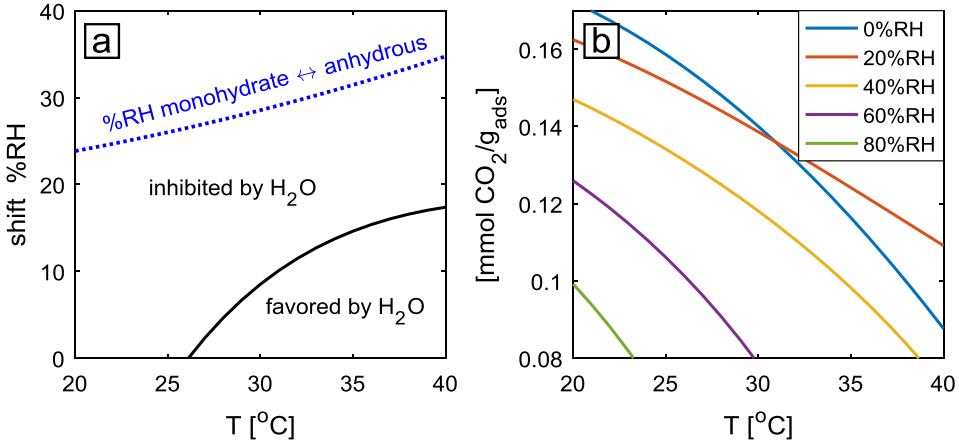


**Fig. 10.** (a) %RH at which the effect of $H_2O$ in the carbonation shifts for a given temperature. (b) Variation of the capture capacity with %RH at different temperatures. The values apply for an adsorbent with a salt loading of 0.042 $g_{Na2CO3}/g_{ads}$.

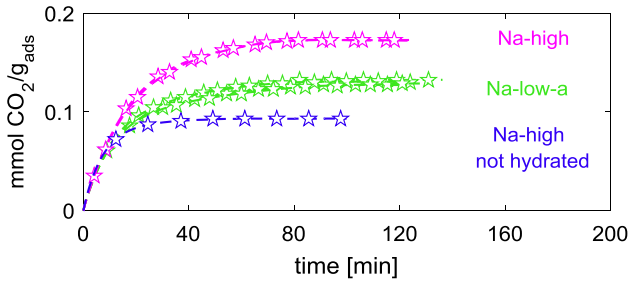


**Fig. 12.** Cumulative capacity of Na-low-a and Na-high with and without pre-hydration. Adsorption conditions were 30 °C, $P_w$ = 11 mbar and F = 10 L/min.

production yield compared to open greenhouses, primarily due to higher $CO_2$ concentrations reached in closed installations (Qian et al., 2011). Currently, $CO_2$ is delivered via the burning of fossil fuels, an alternative to this could be to pump $CO_2$ from outdoors into the greenhouse. Having a greenhouse enclosing 2000 $m^3$ of air and setting the required indoor $CO_2$ concentration to 1200 ppm, the amount of adsorbent needed would be roughly 660 kg. This is based on a $CO_2$ capture capacity of 0.1 mmol $CO_2/g_{ads}$, which showed to be the lower boundary of the tests from the design of experiments set and assuming that the total $CO_2$ enrichment is to be achieved in one single adsorption/desorption cycle. The bulk density of the Na-low-a adsorbent was 420 kg/$m^3$ resulting in an adsorbent volume of 1.6 $m^3$. The ratio of the required adsorbent volume over the total volume of air enclosed in the greenhouse is roughly 0.08%. Loading more salt over the carrier could lead to higher adsorption capacities and consequently to a less amount of adsorbent. Fig. 12 shows the cumulative adsorption capacity of adsorbent Na-high at 30 °C, 11 mbar and 10 L/min. This adsorbent had a salt loading of 0.088 g $Na_2CO_3/g_{ads}$, almost twice that of the first two adsorbents (see Table 1). Although the capture capacity did increase, it was not doubled. This can be partly explained due to mass transfer limitations through a thicker layer of salt. With a capture capacity of 0.15 mmol $CO_2/g_{ads}$ and an adsorbent density of 440 kg/$m^3$, the required amount of adsorbent reduces to 440 kg and the volume ratio to 0.05%. It is also possible to further reduce the amount of adsorbent required if the $CO_2$ enrichment is achieved in batches, provided that two or more adsorption-desorption cycles are run in a brief timeframe to fulfill the daily requirements inside the greenhouse.

Finally, to get an impression of running the desorption step with a mild temperature and moisture swing, two $P_w$ conditions were tested, both at 65 °C and using the Na-high adsorbent. The desorption capacities are shown in Fig. 13. Assuming that the air fed already had 12 mbar $H_2O$ (equivalent to 52%RH at 20 °C) and no extra moisture was added, the desorption capacity was 0.07 mmol $CO_2/g_{ads}$. When the moisture content was raised to $P_w$ = 75 mbar, the desorption capacity increased to 0.1 mmol $CO_2/g_{ads}$. The relatively low temperature requirement to heat the adsorbent to 65 °C and up to 40 °C for a water reservoir to reach 75 mbar

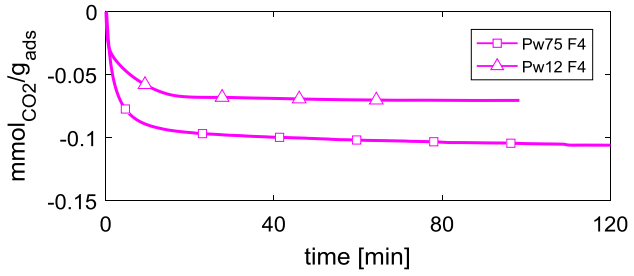


**Fig. 13.** Cumulative desorption capacity of Na-high at 65 °C, F = 4 L/min, under different $P_w$.

(100%RH at 40 °C), suggests that it can easily be fulfilled using solar energy or waste heat. For instance, a volume of warm air (e.g. heated with a solar air heater or with waste heat from an external source) can be recirculated in the reactor until the adsorbent reaches a temperature high enough to prevent water condensation, then the desorption step can be run at the selected temperature and water vapor pressure conditions.

## 4. Conclusions

Adsorbents comprised of $Na_2CO_3$ supported over activated carbon honeycombs are an attractive option for capturing $CO_2$ directly from ambient air. The captured $CO_2$ can be released into greenhouses, enriching the $CO_2$ concentration indoors, thus avoiding the use of $CO_2$ from fossil sources. The adsorbents tested here are cheap, easy to produce and non-hazardous compared to amine-based adsorbents. $Na_2CO_3$ showed to increase the water adsorption of the adsorbent, forming $Na_2CO_3{\cdot}H_2O$. The very low $CO_2$ partial pressure in air limited the total salt conversion into $NaHCO_3$, and the Toth model showed to fit well the experimental data. The hydrated adsorbent was prone to react with air containing 400 ppm $CO_2$ in a wide range of temperature and moisture contents in ambient air. The effects of the temperature, water vapor pressure and flow rate on the $CO_2$ capture were studied following a design of experiments method. The $CO_2$ capture decreased at higher temperatures and moisture contents. These two factors showed interaction with each other, and this defined the conditions at which curvature in the $CO_2$ adsorption performance occurred. Evaporation of water from the pores of the adsorbent enhanced the $CO_2$ capture due to local cooling. The lower adsorption capacity boundary reached of 0.1 mmol $CO_2/g_{ads}$ would result on a volume occupation of roughly 0.08% of the total volume of a closed greenhouse for a $CO_2$ concentration target set at 1200 ppm. A preliminary test showed the feasibility of regenerating the adsorbent with a mild temperature and humidity swing at 65 °C and $P_w$ = 75 mbar under a flush of air. These mild desorption conditions could be fulfilled using waste heat or renewable sources, such as solar heat.

## Acknowledgments

Portions of information contained in this publication are printed with permission of Minitab Inc. All such material remains the exclusive property and copyright of Minitab Inc. All rights reserved. MINITAB® and all other trademarks and logos for the Company's products and services are the exclusive property of Minitab Inc. All other marks referenced remain the property of their respective owners. See minitab.com for more information.

The authors thank Ir. Henk-Jan Moed for his technical contributions.

This research did not receive any specific grant from funding agencies in the public, commercial or not-for-profit sectors.

## Appendix A. Supplementary material

Supplementary data associated with this article can be found, in the online version, at https://doi.org/10.1016/j.ces.2018.05.043.

## References

Sinha, A., Darunte, L.A., Jones, C.W., Realff, M.J., Kawajiri, Y., 2017. Systems design and economic analysis of direct air capture of $CO_2$ through temperature vacuum swing adsorption using MIL-101(Cr)-PEI-800 and mmen-Mg2(dobpdc) MOF Adsorbents. Ind. Eng. Chem. Res. 56 (3), 750–764.

Kulkarni, A.R., Sholl, D.S., 2012. Analysis of equilibrium-based TSA processes for direct capture of $CO_2$ from Air. Ind. Eng. Chem. Res. 51 (25), 8631–8645.

Tran, P.D., Wong, L.H., Barber, J., Loo, J.S.C., 2012. Recent advances in hybrid photocatalysts for solar fuel production. Energy Environ. Sci. 5 (3), 5902–5918.
Smestad, G.P., Steinfeld, A., 2012. Review: photochemical and thermochemical production of solar fuels from $H_2O$ and $CO_2$ using metal oxide catalysts. Ind. Eng. Chem. Res. 51 (37), 11828–11840.
Holmes, G., Nold, K., Walsh, T., Heidel, K., Henderson, M.A., Ritchie, J., Klavins, P., Singh, A., Keith, D.W., 2013. Outdoor prototype results for direct atmospheric capture of carbon dioxide. Energy Procedia 37, 6079–6095.
Mahmoudkhani, M., Heidel, K.R., Ferreira, J.C., Keith, D.W., Cherry, R.S., 2009. Low energy packed tower and caustic recovery for direct capture of $CO_2$ from air. Energy Procedia 1 (1), 1535–1542.
Mahmoudkhani, M., Keith, D.W., 2009. Low-energy sodium hydroxide recovery for $CO_2$ capture from atmospheric air—Thermodynamic analysis. Int. J. Greenh. Gas Control 3 (4), 376–384.
Wang, T., Lackner, K.S., Wright, A., 2011. Moisture swing sorbent for carbon dioxide capture from ambient air. Environ. Sci. Technol. 45 (15), 6670–6675.
Shi, X., Li, Q., Wang, T., Lackner, K.S., 2017. Kinetic analysis of an anion exchange absorbent for CO2 capture from ambient air. PLOS ONE, 12, (6), e0179828.
Choi, S., Drese, J.H., Eisenberger, P.M., Jones, C.W., 2011. Application of amine-tethered solid sorbents for direct $CO_2$ Capture from the ambient air. Environ. Sci. Technol. 45 (6), 2420–2427.
Choi, S., Gray, M.L., Jones, C.W., 2011. Amine-tethered solid adsorbents coupling high adsorption capacity and regenerability for $CO_2$ capture from ambient air. ChemSusChem 4, 628–635.
Brilman, W.F., Veneman, R., 2013. Capturing atmospheric $CO_2$ using supported amine sorbents. Energy Procedia 37, 6070–6078.
Chaikittisilp, W., Khunsupat, R., Chen, T.T., Jones, C.W., 2011. Poly(allylamine)–mesoporous silica composite materials for $CO_2$ capture from simulated flue gas or ambient air. Ind. Eng. Chem. Res. 50 (24), 14203–14210.
Belmabkhout, Y., Serna-Guerrero, R., Sayari, A., 2010. Amine-bearing mesoporous silica for $CO_2$ removal from dry and humid air. Chem. Eng. Sci. 65, 3695–3698.
Wurzbacher, J.A., Gebald, C., Piatkowski, N., Steinfeld, A., 2012. Concurrent separation of $CO_2$ and $H_2O$ from air by a temperature-vacuum swing adsorption/desorption cycle. Environ. Sci. Technol. 46 (16), 9191–9198.
Zhang, W., Liu, H., Sun, C., Drage, T.C., Snape, C.E., 2014. Capturing CO2 from ambient air using a polyethyleneimine–silica adsorbent in fluidized beds. Chem. Eng. Sci. 116, (Supplement C), 306–316.
Sanz-Pérez, E.S., Murdock, C.R., Didas, S.A., Jones, C.W., 2016. Direct capture of $CO_2$ from ambient air. Chem. Rev. 116 (19), 11840–11876.
Sakwa-Novak, M.A., Yoo, C.J., Tan, S., Rashidi, F., Jones, C.W., 2016. Poly (ethylenimine)-functionalized monolithic alumina honeycomb adsorbents for $CO_2$ capture from air. ChemSusChem 9 (14), 1859–1868.
Derevschikov, V.S., Veselovskaya, J.V., Kardash, T.Y., Trubitsyn, D.A., Okunev, A.G., 2014. Direct $CO_2$ capture from ambient air using $K_2CO_3/Y_2O_3$ composite sorbent. Fuel 127, 212–218.
Veselovskaya, J.V., Derevschikov, V.S., Kardash, T.Y., Stonkus, O.A., Trubitsina, T.A., Okunev, A.G., 2013. Direct $CO_2$ capture from ambient air using $K_2CO_3/Al_2O_3$ composite sorbent. Int. J. Greenh. Gas Control 17, 332–340.
Vanderzee, C.E., 1982. Thermodynamic relations and equilibria in ($Na_2CO_3$ + $NaHCO_3$ + $H_2O$): standard Gibbs energies of formation and other properties of sodium hydrogen carbonate, sodium carbonate heptahydrate, sodium carbonate decahydrate, trona: ($Na_2CO_3{\cdot}NaHCO_3{\cdot}2H_2O$), and Wegscheider's salt: ($Na_2CO_3{\cdot}3NaHCO_3$). J. Chem. Thermodyn. 14 (3), 219–238.
Vanderzee, C.E., Wigg, D.A., 1981. The standard enthalpies of solution and formation of Wegscheider's salt: $Na_2CO_3 \cdot 3NaHCO_3$(s) and of trona: $Na_2CO_3 \cdot NaHCO_3 \cdot 2H_2O$(s) at 298.15 K. J. Chem. Thermodyn. 13 (6), 573–583.
Wong, S.C., 1990. Elevated atmospheric partial pressure of $CO_2$ and plant growth: II. Non-structural carbohydrate content in cotton plants and its effect on growth parameters. Photosynth. Res. 23 (2), 171–180.
Pritchard, S.G., Rogers, H.H., Prior, S.A., Peterson, C.M., 1999. Elevated $CO_2$ and plant structure: a review. Global Change Biology 5 (7), 807–837.
Brunauer, S., Emmett, P.H., Teller, E., 1938. Adsorption of gases in multimolecular layers. J. Am. Chem. Soc. 60 (2), 309–319.
Barrett, E.P., Joyner, L.G., Halenda, P.P., 1951. The determination of pore volume and area distributions in porous substances. I. computations from nitrogen isotherms. J. Am. Chem. Soc. 73 (1), 373–380.
Do, D.D., Junpirom, S., Do, H.D., 2009. A new adsorption–desorption model for water adsorption in activated carbon. Carbon 47 (6), 1466–1473.
Tedds, S., Walton, A., Broom, D.P., Book, D., 2011. Characterisation of porous hydrogen storage materials: carbons, zeolites MOFs and PIMs. Faraday Discuss. 151, 75–94.
Tanaka, H., 1987. Comparison of thermal properties and kinetics of decompositions of $NaHCO_3$ and $KHCO_3$. J. Therm. Anal. 32 (2), 521–526.
Buijs, K., Schutte, C.J.H., 1961. The infra-red spectra and structures of $Li_2CO_3$ and anhydrous $Na_3CO_3$. Spectrochim. Acta 17 (9), 927–932.
Apelblat, A., Manzurola, E., 2003. Solubilities and vapour pressures of saturated aqueous solutions of sodium tetraborate, sodium carbonate, and magnesium sulfate and freezing-temperature lowerings of sodium tetraborate and sodium carbonate solutions. J. Chem. Thermodyn. 35 (2), 221–238.
Buijs, K., Schutte, C.J.H., 1961. An infra-red study of the hydrates of sodium carbonate. Spectrochim. Acta 17 (9), 917–920.
De Gelder, A., Dieleman, J.A., Bot, G.P.A., Marcelis, L.F.M., 2012. An overview of climate and crop yield in closed greenhouses. J. Hortic. Sci. Biotechnol. 87 (3), 193–202.
Qian, T., Dieleman, J.A., Elings, A., De Gelder, A., Marcelis, L. F.M., Van Kooten, O., 2011. In Comparison of climate and production in closed, semi-closed and open greenhouses, 2011; International Society for Horticultural Science (ISHS), Leuven, Belgium: pp 807–814